Turkish Journal of Agriculture and Forestry

Volume 48 | Number 3 Article 9

6-6-2024

Photovoltaic fault detection based on infrared and visible image augmentation and fusion

XUEWEI CHAO

LIXIN ZHANG

YANG LI

CHAO HUANG

JING LI

Recommended Citation

CHAO, XUEWEI; ZHANG, LIXIN; LI, YANG; HUANG, CHAO; and LI, JING (2024) "Photovoltaic fault detection based on infrared and visible image augmentation and fusion," *Turkish Journal of Agriculture and Forestry*: Vol. 48: No. 3, Article 9. https://doi.org/10.55730/1300-011X.3192
Available at: https://journals.tubitak.gov.tr/agriculture/vol48/iss3/9

Turkish Journal of Agriculture and Forestry

http://journals.tubitak.gov.tr/agriculture/

Research Article

Turk J Agric For
(2024) 48: 430-442

doi:10.55730/1300-011X.3192

Photovoltaic fault detection based on infrared and visible image augmentation and fusion

Xuewei CHAO[1], Lixin ZHANG[1,2,*], Yang LI[1], Chao HUANG[1], Jing LI[1]
[1]College of Mechanical and Electrical Engineering, Shihezi University, Shihezi, China
[2]Bingtuan Energy Development Institute, Shihezi University, Shihezi, China

Received: 13.03.2024 • **Accepted/Published Online:** 26.04.2024 • **Final Version:** 06.06.2024

Abstract: The rapid development of the agricultural photovoltaic integration model holds significant importance in improving land utilization and the economic benefits of green energy. However, due to the harsh working environment and prolonged exposure to natural conditions, photovoltaic (PV) components are prone to hot spot faults, leading to severe consequences. In this article, we propose a fine-grained PV hot spot fault detection framework based on the fusion of infrared and visible light images, addressing various factors that contribute to hot spot faults. Firstly, we collected multiple sets of infrared and visible light image pairs under different hot spot fault conditions. We employed generative adversarial networks (GANs) to augment the collected infrared-visible light image pairs, effectively expanding the dataset. Subsequently, we applied data augmentation techniques to further increase the data volume. To eliminate information redundancy caused by data augmentation, we introduce a novel information quality evaluation method called cosine distance pseudo-label cross-entropy (CDPC). This method enables the selection of high-quality infrared-visible light image pairs for model training and fine-grained fault detection. Experimental results demonstrate the stability and effectiveness of the proposed detection method based on information fusion, with an average testing accuracy of 93.7% for fine-grained fault recognition. Moreover, the efficiency of data training is significantly improved. Taking 35% of the whole training data as an example, the recognition accuracy trained with high-quality data is nearly 12% higher than that trained with low-quality data. Furthermore, under the premise of the same accuracy, the used dataset can be compressed by 30%, effectively reducing the model training time and carbon emission.

Key words: Data expansion, information fusion, quality evaluation, photovoltaic failure, fault detection

1. Introduction

Due to the global climate and energy crisis, the importance of sustainable development has become increasingly evident, leading to widespread attention in the research of carbon emission reduction and carbon neutrality (Sovacool and Griffiths, 2020; You et al., 2022). In the context of sustainable agricultural development, the integration of agriculture and photovoltaics is emerging as a highly promising green energy solution. This approach combines photovoltaic power generation with agricultural cultivation, allowing for the generation of electricity resources without affecting the normal growth of crops. It provides energy supply for agricultural field management while saving land area for photovoltaic installations. This enhances the utilization of land resources and has a positive impact on providing renewable energy and adding value to farmland (Nie et al., 2022a; Li et al., 2022a; Yang et al., 2022b; Nie et al., 2022b). In the agricultural photovoltaic integration model, the photovoltaic systems are typically installed in idle areas of farmland or farms, as shown in Figure 1. This installation approach maximizes the utilization of land resources without compromising regular agricultural activities. It also supplies renewable electricity to support agricultural operations, thereby promoting the electrification process in the agricultural sector. Furthermore, the agricultural photovoltaic integration model can create value-added services for agriculture. The installation of photovoltaic systems can generate additional income for farms, enhancing their economic benefits and providing more opportunities for sustainable agricultural development. However, considering the complex and diverse agricultural production environment, it is inevitable for photovoltaic modules to experience various failures after prolonged exposure to harsh conditions. These failures may include broken glass, damaged batteries, plant obstructions, abnormal covers, short circuits, and surface contamination, as depicted in Figure 2 (Hernández-Callejo et al., 2019). Such failures can disrupt the stability of photovoltaic power generation, leading to reduced electricity production and potential

* Correspondence: shzujd@163.com

Figure 1. Agricultural photovoltaic combined development scenario.

Figure 2. Photovoltaic systems exposed to complex environments in farmland.

safety risks. Hence, it is of utmost importance to promptly identify and classify different types of hot spot faults in photovoltaic systems. This enables repair personnel to quickly conduct necessary repairs, ensuring continuous electricity production and mitigating safety hazards.

In order to improve the working stability of photovoltaic modules, the intelligent fault diagnosis studies of photovoltaic modules are necessary, which mainly include electrical performance evaluation and image recognition, the former is based on voltage and current characteristics, which is accurate but inefficient, the latter is to extract image features based on deep learning and establish fault patterns mapping relationship. Specifically, deep learning-based image identification techniques require less labor and are more efficient than electrical testing methods (Li et al., 2021); thus, deep learning-based image processing methods are more suitable for the rapidly evolving photovoltaic module fault detection tasks. However, as a typical data-hungry machine learning paradigm, deep learning requires a large amount of labeled data for training, which will bring in serious data efficiency problems (Li et al., 2020; Khan et al., 2022; Alghazzawi et al., 2022). For instance, too much similar data without incremental information contribution will increase the training time of the used model and further increase power consumption and carbon emissions, which is not sustainable. To solve this matter, there have been several data quality evaluation studies in the field of deep learning applications (Li and Chao, 2022; Li et al., 2022b; Yang et al., 2022a; Yang et al., 2023a), which focus on screening high-quality image samples, reducing database redundancy, and improving task performance and efficiency.

In terms of photovoltaic module hot spot image identification, some recent relevant studies (Wang and Xuan, 2021; Ali et al., 2020; Ghosh et al., 2020; Su et al., 2021) conducted the pattern recognition based on infrared images because the hot spot fault is a kind of thermal effect, and the fault area has a significant temperature difference with the normal area, resulting in color differences in infrared imaging. The presence of fine-grained fractures

within a photovoltaic system has detrimental effects, including energy loss, decreased power generation efficiency, and potential impact on the system's overall lifespan. Implementing fine-grained detection techniques plays a crucial role in identifying and recognizing efficiency losses, precisely locating fault points, and undertaking suitable measures to enhance the performance of the photovoltaic system while extending its operational lifespan. By effectively addressing these fractures, the system's energy production can be optimized, leading to improved efficiency and prolonged functionality (Dhoke et al., 2020; Malik et al., 2022). However, the hot spot fault of photovoltaic modules may have a variety of causes, such as circuit failure, guano dirt coverage, and shadow occlusion, and different cases of hot spot faults correspond to different treatments. For example, the short circuit fault needs to be repaired or replaced, the dirt cover fault needs to be cleaned, and the shading fault requires adjustment of photovoltaic panel spacing or angle. Therefore, it is very rough to only make the binary classification on whether hot spot fault occurs, which is not conducive to practical applications or production maintenance.

The motivation of this paper is clear, which aims at this meaningful problem. We propose to combine the dual heterogeneous information of infrared and visible images to carry out the research of fine-grained hot spot fault recognition. As far as we know, this is the first time to conduct fine-grained detection work for photovoltaic module hot spot failures. Some related works in heterogeneous data processing cover many fields, such as medicine, agriculture, and industry (Xie et al., 2021; Zhang et al., 2021; Tang et al., 2022; Li et al., 2022c; Patil and Kumar, 2022), which often involve data feature extraction, alignment, and fusion. In general, the combination of heterogeneous data will improve the performance of various tasks because the heterogeneous data can provide additional information that single modal data could not.

In this paper, infrared and visible images of photovoltaic module hot spot fault were collected, and fine-grained labels were manually marked. Since the heterogeneous images are required as input, the infrared and visible images are bundled and appear in pairs with the same label. Next, a fine-grained detection framework of hot spot fault based on infrared and visible image fusion was established. Subsequently, a data information quality evaluation method named cosine distance pseudo-label cross-entropy (CDPC) was designed to reduce data redundancy and screen out high-quality samples. Finally, the dimensionality reduction for fusional image feature was conducted to detect fine-grained hot spot faults. Through a large number of comparative experiments, the results show that the proposed fine-grained framework is effective and achieves 93.7% detection accuracy. Under the premise of the same accuracy, the used dataset can be compressed by 30%, effectively reducing the training time and carbon emission.

This study collected paired infrared and visible images of photovoltaic module hot spot faults and manually annotated fine-grained labels. Since heterogeneous images are required as inputs, the infrared and visible images were bundled together and appeared in pairs with the same labels. Subsequently, the collected infrared-visible image pairs were augmented using a generative adversarial network (GAN), and data augmentation methods were employed to further expand the dataset. A fine-grained hot spot fault detection framework based on the fusion of infrared and visible images was then established. Additionally, a cosine distance pseudo-label cross-entropy (CDPC) method was designed to evaluate the information quality of the data, aiming to reduce redundancy and select high-quality samples. Finally, the fused image features were dimensionally reduced to detect fine-grained hot spot faults. Extensive comparative experiments demonstrated that the proposed fine-grained framework was effective, achieving a detection accuracy of 93.7%. Furthermore, under the same level of accuracy, the utilized dataset could be compressed by 30%, effectively reducing training time and carbon emissions.

The rest of this paper is organized as follows. Section 2, presents the collected fine-grained hot spot fault dataset and introduces the proposed data quality assessment method. Section 3 conducts comparison experiments and analyzes the results. Section 4 discusses the motivations, main works, core contributions, limitations, and future works. Finally, Section 5 provides a summary of the entire study.

2. Materials and methods

2.1. Dataset

In order to recognize the fine-grained hot spot faults of photovoltaic modules caused by different factors, we collected 6 types of hot spot failures in the agricultural PV development region, covering visible and infrared images at the same time, and presenting them in the form of image pairs. Some image pair samples are shown in Figure 3, where the fine-grained fault types include broken glass, broken battery, plant occlusion, abnormal cover, short circuit, and surface contamination.

Due to the complex and harsh environment in which photovoltaic operations are carried out, conducting data collection of each individual photovoltaic panel would significantly increase the cost of data acquisition and decrease efficiency. It would also cause irreversible impacts on crops in the environment. Collecting a sufficient number of data samples from photovoltaic systems in agricultural planting areas may present challenges. However, at the same time, data samples are an important factor affecting the accuracy of photovoltaic fault detection. To address the issue of insufficient data samples

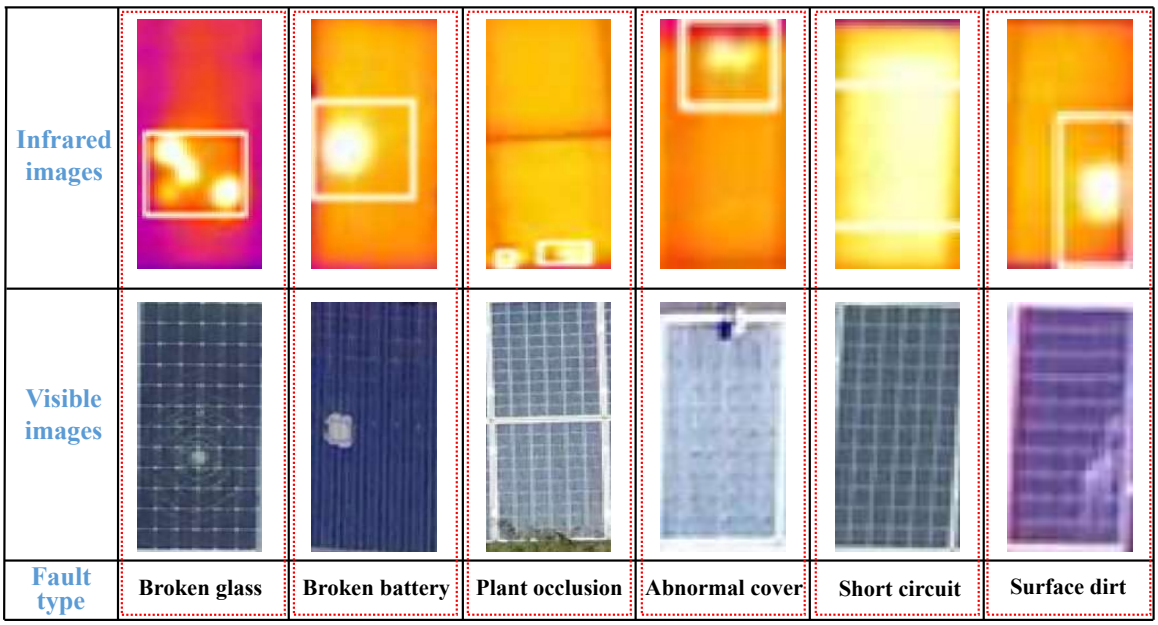

Figure 3. Samples of the dual-modal image pairs for fine-grained hot spot fault.

in the PV fault image dataset and optimize the agricultural PV integration development model, this study employs generative adversarial networks (GANs) to enhance the collected infrared-visible image pairs of PV faults in the field. By utilizing existing data samples, we can generate more synthetic data samples to improve the efficiency and accuracy of photovoltaic fault detection, while reducing environmental impact and data acquisition costs. Subsequently, traditional data augmentation methods are applied to optimize the samples, effectively addressing the problem of imbalanced data distribution in the PV fault image dataset. This approach improves the model's generalization ability and reduces the risk of overfitting.

To better adapt to the photovoltaic fault detection process in agricultural production scenarios, improve the accuracy of photovoltaic fault detection, and ensure the normal operation of photovoltaic systems, this paper proposes an infrared-visible bundled generation model. The visible photovoltaic fault images and infrared photovoltaic fault images are defined as domain V and domain S, respectively. The model structure is shown in Figure 4.

The infrared-visible bundled generation augmentation model is based on a pair of generative adversarial networks (GANs), namely the visible-to-infrared image GAN (GAN_{VS}) and the infrared-to-visible image GAN (GAN_{SV}). Both the infrared image generator (G_{VS}) and the visible image generator (GSV) have the same structure, consisting of five convolutional blocks. Each convolutional block includes a convolutional layer, a batch normalization layer, and a rectified linear unit (ReLU) activation function layer. The convolutional layer comprises numerous convolutional filters that conduct convolutional operations on the input data, resulting in the creation of a collection of feature maps. Each feature map corresponds to a specific learned feature captured by a convolutional filter, thereby facilitating the extraction of distinctive features from the input data. Through this process, the convolutional layer effectively identifies and highlights relevant patterns and structures within the input, enabling subsequent layers in the network to make more informed and accurate predictions or decisions based on the extracted features. In essence, the convolutional layer acts as a feature extractor, transforming the raw input data into a representation that captures important visual characteristics. The batch normalization layer normalizes the output of each convolutional layer, making the output have zero mean and unit variance, which helps the network converge faster and improves the model's robustness. The ReLU activation function layer introduces nonlinear transformations by mapping the output of the convolutional layer nonlinearly, thereby enhancing the expressive power of the network. The kernel sizes of the first and second convolutional blocks are set as 7×7 and 5×5, respectively, indicating larger receptive fields for feature extraction. The kernel sizes of the third and fourth convolutional blocks are set as 3×3, favoring optimization of the feature maps. The kernel size of the last convolutional block is set as 1×1, primarily used for dimension reduction, ensuring the generated images have the desired color channels.

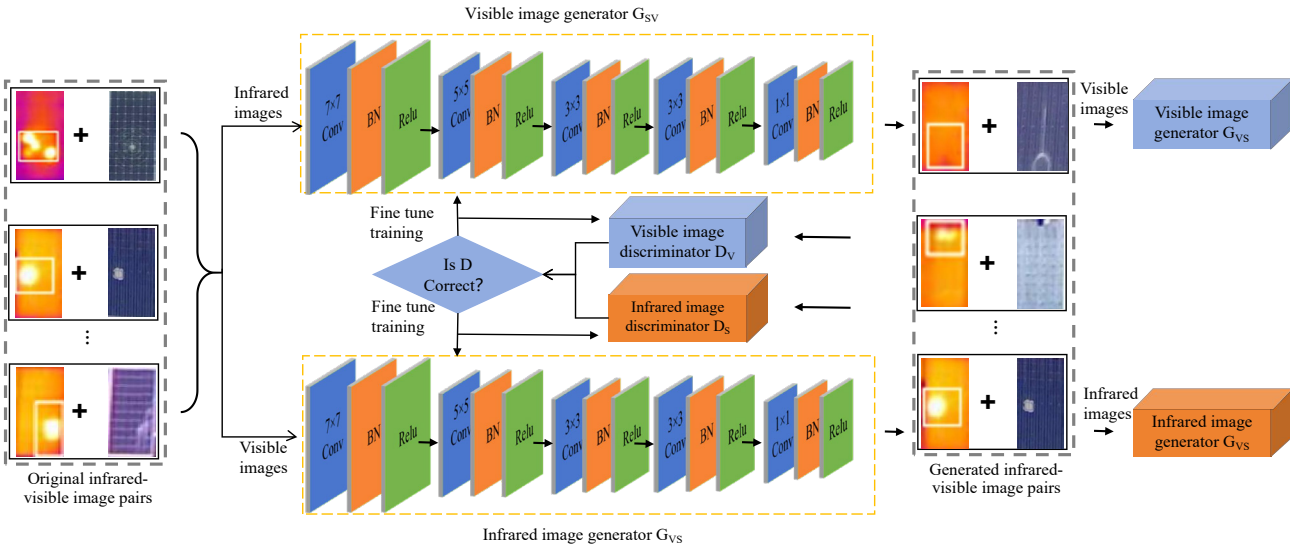

Figure 4. Infrared-visible bundled generation model.

The generator network takes pairs of collected images as input and generates corresponding images. Simultaneously, the discriminator network distinguishes between the generated images from the generator network and real images. Through iterative training, the discriminator's feedback is utilized to update both the generator and discriminator networks. The generator gradually learns how to generate realistic output images from the input images, while the discriminator learns how to accurately determine the authenticity of input images. The specific steps of the bundled generation augmentation method are as follows:

Step 1: Input infrared-visible image pairs: A pair of infrared-visible images collected from the agricultural field, which demonstrate a corresponding relationship, are provided as input to the generator network.

Step 2: Generate visible and infrared images: The G_{SV} generates the corresponding visible image from the input infrared image, and the G_{VS} generates the corresponding infrared image from the input visible image.

Step 3: Discriminate visible and infrared images: The D_S judges the generated infrared image against the real infrared image and calculates the loss between them. Similarly, the D_V judges the generated visible image against the real visible image and calculates the loss between them.

Step 4: Update the generator: The G_{SV} updates itself by minimizing the loss calculated by the D_V for the generated visible image. Similarly, the G_{VS} updates itself by minimizing the loss calculated by the D_S for the generated infrared image.

Step 5: Update the discriminator: The D_S updates itself by maximizing the log probability of correctly judging real infrared images and the negative log probability of correctly judging generated infrared images. Similarly, the D_V updates itself by maximizing the log probability of correctly judging real visible images and the negative log probability of correctly judging generated visible images.

Step 6: Generate new image pairs: After training, the generator network gains the ability to produce corresponding images for any input image. This enables the creation of new image pairs, expanding the training dataset. These generated pairs resemble real images, adding diversity and enhancing the model's generalization. By incorporating these realistic image pairs during training, the model learns from a wider range of examples, improving its performance on unseen data. This augmentation enriches the dataset, introducing variations that enhance the model's robustness in handling different scenarios.

The training process of the model requires a loss function to measure the performance of the generator and discriminator networks while guiding the training process. The loss function of this model includes adversarial loss, cycle consistency loss, identity loss, and antirecovery consistency loss. The adversarial loss is primarily used to quantify the difference between the generated images and real images. The cycle consistency loss ensures that the generator can achieve bidirectional mapping, meaning that the generated visible image (infrared image) can be faithfully restored to the original infrared image (visible image) through the infrared image generator G_{VS} (visible image generator G_{SV}). The identity loss aims to maintain the stability of the generator by encouraging the generator to faithfully reproduce the original image when the original image is passed through the generator. The anti-recovery consistency loss encourages the generator not to fully

recover the original image during the cycle conversion, resulting in some differences in the generated image pairs. By adjusting the weights of these loss terms in the overall loss function, the model generates image pairs with certain differences from the original image pairs, thereby achieving data augmentation. The specific formulas are as follows:

Adversarial loss is shown in Eqs. (1) and (2).

$$L_{GAN(Gsv,Dv,S,V)} = E\left[\log(Dv(V))\right] + E\left[\log(1 - Dv(Gsv(S)))\right] \cdot \quad (1)$$

$$L_{GAN(Gvs,Ds,V,S)} = E\left[\log(Ds(S))\right] + E\left[\log(1 - Ds(Gvs(V)))\right] \cdot \quad (2)$$

where $L_{GAN(GSV,DV,S,V)}$ and $L_{GAN(GVS,DS,V,S)}$ are the adversarial loss functions for infrared-to-visible and visible-to-infrared, respectively. Furthermore, E represents the expected value.

Cycle consistency loss is shown in Eqs. (3) and (4).

$$L_{cycle(Gsv,Gvs,S,V)} = E\left[\left\|Gvs(Gsv(S))\text{-}S\right\|_1\right] + E\left[\left\|Gsv(Gvs(V))\text{-}V\right\|_1\right] \cdot \quad (3)$$

$$L_{cycle(Gvs,Gsv,V,S)} = E\left[\left\|Gsv(Gvs(V))\text{-}V\right\|_1\right] + E\left[\left\|Gvs(Gsv(S))\text{-}S\right\|_1\right] \cdot \quad (4)$$

where $L_{cycle(GSV,DV,S,V)}$ and $L_{cycle(GVS,DS,V,S)}$ are the cycle consistency loss functions for infrared-to-visible and visible-to-infrared, respectively.

Identity loss is shown in Eqs. (5) and (6).

$$L_{identity(Gsv,Gvs,S,V)} = E\left[\left\|(Gvs(V))\text{-}V\right\|_1\right] + E\left[\left\|(Gsv(S))\text{-}S\right\|_1\right] \cdot \quad (5)$$

$$L_{identity(Gvs,Gsv,V,S)} = E\left[\left\|(Gsv(S))\text{-}S\right\|_1\right] + E\left[\left\|(Gvs(V))\text{-}V\right\|_1\right] \cdot \quad (6)$$

where $L_{identity(GSV,DV,S,V)}$ and $L_{identity(GVS,DS,V,S)}$ are the identity loss functions for infrared-to-visible and visible-to-infrared, respectively.

Antirecovery consistency loss is shown in Eqs. (7) and (8).

$$L_{antirecovery(Gsv,Gvs,S,V)} = E\left[\left\|(Gsv(Gvs(Gsv(S))) - Gsv(S)\right\|_1\right] \cdot \quad (7)$$

$$L_{antirecovery(Gvs,Gsv,V,S)} = E\left[\left\|(Gvs(Gsv(Gvs(V))) - Gvs(V)\right\|_1\right] \cdot \quad (8)$$

where $L_{adtirecovery\ (GSV,DV,S,V)}$ and $L_{adtirecovery\ (GVS,DS,V,S)}$ are the antirecovery consistency loss functions for infrared-to-visible and visible-to-infrared, respectively.

Objective function is shown in Eq (9).

$$\begin{aligned} L = {} & \lambda_{GANsv} \times L_{GAN(Gsv,Dv,S,V)} + \lambda_{GANvs} \times L_{GAN(Gvs,Ds,V,S)} \\ & + \lambda_{cycle(Gsv,Gvs,S,V)} \times L_{cycle(Gsv,Gvs,S,V)} + \lambda_{cycle(Gvs,Gsv,V,S)} \times L_{cycle(Gvs,Gsv,V,S)} \\ & + \lambda_{identity(Gsv,Gvs,S,V)} \times L_{identity(Gsv,Gvs,S,V)} + \lambda_{identity(Gvs,Gsv,V,S)} \times L_{identity(Gvs,Gsv,V,S)} \\ & + \lambda_{antirecovery(Gsv,Gvs,S,V)} \times L_{antirecovery(Gsv,Gvs,S,V)} + \lambda_{antirecovery(Gvs,Gsv,V,S)} \times L_{antirecovery(Gvs,Gsv,V,S)} \end{aligned} \quad (9)$$

where λ represents the weight coefficients for each loss term.

In this study, the original dataset was collected from a pilot project on agricultural-photovoltaic integration. After collecting the images, they underwent normalization processing, resulting in an image resolution of 300×600. From this dataset, a total of 120 pairs of visible light-infrared images were selected, encompassing six types of photovoltaic faults: broken glass, broken battery, plant occlusion, abnormal cover, short circuit, and surface contamination. Among these pairs, 100 were used for training, while 20 pairs were reserved for testing purposes. To enhance the training dataset, the collected image data undergoes Cycle GAN to increase the number of image pairs in each category to 500. Furthermore, data augmentation techniques are applied, expanding the dataset to contain 1000 image pairs per category. These techniques involve operations like mirroring, contrast adjustment, rotation, and scaling. By employing these augmentation methods, the dataset becomes more diverse, offering a wider range of examples and improving the model's ability to handle various scenarios effectively.

2.2. Fine-grained hot spot fault detection framework

The occurrence mechanism of hot spot faults causes them to be clearly reflected in infrared images. However, different kinds of hot spot faults cannot be clearly distinguished from infrared images only, and the auxiliary information of visible images are important. Photovoltaic fault detection commonly involves using both infrared and visible light images, which complement each other. Infrared images capture temperature distribution, revealing anomalies caused by damage, poor contacts, or blockages. Visible light images provide information about surface morphology and color, detecting issues like cracks, contamination, or corrosion. Integrating these image types enables comprehensive fault detection and localization. By combining them, faults can be accurately assessed, allowing for timely interventions and ensuring the photovoltaic system's optimal performance and reliability. Therefore, this paper proposes a fine-grained infrared-visible image fusion hot spot fault detection framework, as shown in Figure 5.

The whole framework is divided into two stages. The first stage is to evaluate the quality of the input image pairs to screen out high-quality infrared and visible samples with rich information, and carry out feature extraction by CNN model. In the second stage, the global average pooling (GAP) operation is conducted on the stacked features. Subsequently, the high-dimensional fusional embeddings are reduced in dimension by principal component analysis (PCA) to obtain informative fusional features, which are finally fed into the classifier to carry out fine-grained hot spot fault classification into 6 categories.

2.3. Cosine distance pseudo-label cross-entropy

Visible-infrared image pairs are extensively used in photovoltaic fault detection as a prevalent data format. Evaluating paired data involves assessing visible and infrared images simultaneously, leading to accurate and reliable results. However, this approach requires obtaining and aligning both types of images. In contrast, unpaired data evaluation independently evaluates visible and infrared images, simplifying the data acquisition process but potentially compromising evaluation accuracy. When

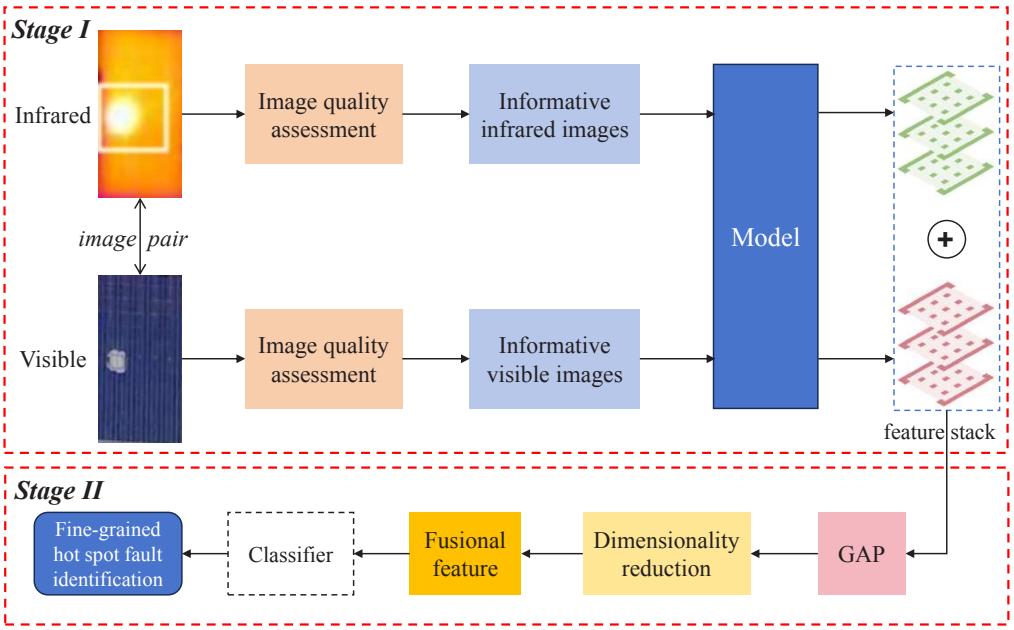

Figure 5. The fine-grained hot spot fault detection framework.

selecting an evaluation method, careful consideration of factors such as feasibility, cost, and accuracy requirements is crucial. By weighing these factors, an optimal evaluation approach can be chosen to achieve effective photovoltaic fault detection. In this paper, we propose a novel image data information quality evaluation method called cosine distance pseudo-label cross-entropy (CDPC), which is referred to as the image quality assessment module in Figure 5. Since infrared and visible images appear in pairs in this work, the proposed quality assessment method evaluates image pairs, which is different from many existing methods (Schlett et al., 2022; Madhusudana et al., 2022; Yang et al., 2023b; Li and Ercisli, 2023).

The workflow of the proposed CDPC image pair quality evaluation method is shown in Figure 6.

Specifically, there are six categories of fine-grained photovoltaic hot spot failures, each of which contains 1000 infrared-visible bundled image pairs, totaling 6000 pairs. These image pairs were randomly divided into the base set and the pool set at 5% and 95%, respectively. Furthermore, the image pairs in the pool set were evaluated and screened, and the samples in the base set were used to fine-tune the feature extractor. Taking an image pair as an example, the pair was fed to the model to extract its feature maps, and the two feature maps were stacked and average pooled as the new feature embedding representing the image pair. In this way, the categorical feature prototypes were obtained by taking average of all the sample pairs in the base set. Then, the stacked features of the image pairs in the pool set were extracted by the model in the same way, using shared parameters for evaluation. Here, the cosine distance between each prototype and the image pair was calculated to obtain the similarity score between the evaluated image pair and each class.

Considering two stacked high-dimensional feature vectors A (a1, a2, ..., an) and B (b1, b2, ..., bn), the cosine distance is calculated according to Eq. (10).

$$cos(\mathrm{A,B}) = \frac{A \cdot B}{\|A\| \times \|B\|} = \frac{\sum_{i=1}^{n} A_i B_i}{\sqrt{\sum_{i=1}^{n} A_i^2}\sqrt{\sum_{i=1}^{n} B_i^2}}. \quad (10)$$

In the equation, *cos* (A, B) represents the cosine distance between feature vector A and feature vector B.

The corresponding pseudolabel was determined according to the similarity score, and the higher the similarity, the more likely it would be because their feature space mapping positions were very close. In addition, the stacked feature vector was also fed to the classifier to predict the probability. Finally, the predicted probability and the pseudolabel were used together to calculate the cross-entropy as the indicator of uncertainty of the infrared-visible image pair, denoted as CDPC loss and expressed as Eq (11).

$$L = -\sum_{i=1}^{M}\left[\hat{y}_i \cdot \log(p_i) + (1-\hat{y}_i)\cdot \log(1-p_i)\right]. \quad (11)$$

Note that the above process can completely sort the image pairs in the pool set and screen out high-value sample pairs based on the CDPC loss, also known as uncertainty. However, the data information quality is a dynamic evolution process, along with the learning of the neural network, it is necessary to update and filter high-

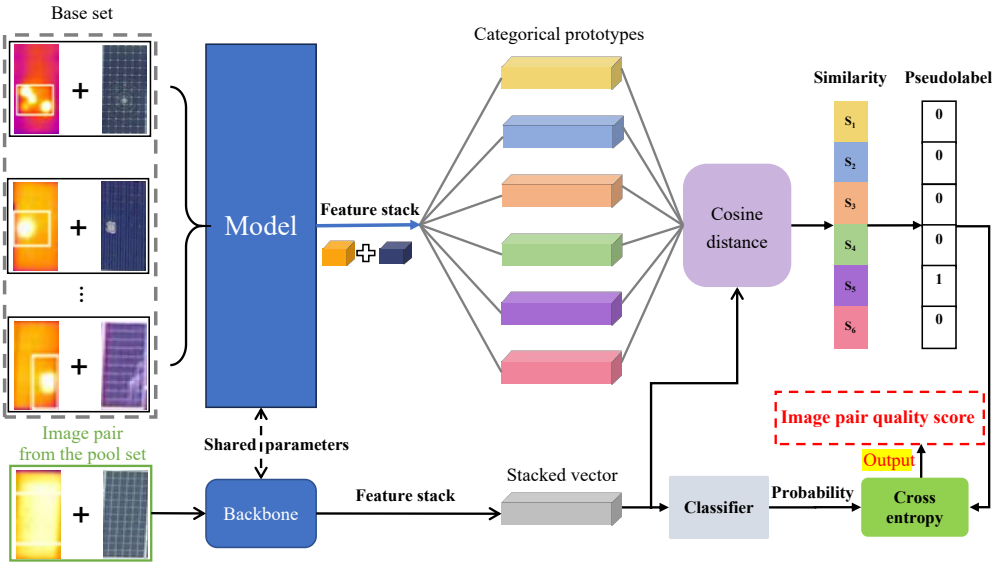

Figure 6. The workflow of the CDPC image pair quality evaluation method.

information image pairs in batches. In this work, 5% of the step size is adopted to screen out high-information image pairs and add them to the base set, and then the whole process is updated to evaluate and screen the pool set to supplement the base set. Lastly, once the data budget of image pairs is reached, the updated base set is output as the screened high-information data consisting of infrared images and visible images.

3. Results and analysis

3.1. Experimental setup

In this study, there are six types of fine-grained photovoltaic hot spot defects, including glass breakage, battery breakage, plant occlusion, abnormal coverage, short circuit, and surface contamination. To enhance the detection performance, the data samples used in the study consist of visible light-infrared image pairs generated using generative adversarial networks and data augmentation methods. These measures were employed to improve the effectiveness of identification and detection in the study. Each type comprises 1000 infrared-visible training image pairs, totaling 6000 pairs in the entire training dataset. Data augmentation is adopted in image preprocessing, which enlarges the experimental setup of the training data scale and inevitably increases the data redundancy.

The study utilizes a framework, shown in Figures 5 and 6, that incorporates well-established CNN models known for their exceptional feature extraction capabilities in image analysis. These models have been extensively validated across diverse domains, affirming their credibility and effectiveness. Additionally, to evaluate the universal applicability of the proposed image pair evaluation method, the study plans to conduct ablation experiments exploring various network architectures. These experiments aim to comprehensively investigate the performance and versatility of the evaluation method in different scenarios, providing valuable insights into its potential benefits.

The image pairs in the used dataset are randomly divided into the base set and the pool set, according to the ratio of 5% and 95%. When the data pair quality assessment based on CDPC starts, the step size is 10%, and the recognition accuracies based on infrared image fusion with different data pair quality are compared until the data budget of 65% of the whole training set is reached. Moreover, each group experiment is repeated 5 times to take the average accuracy as the result, reducing the influence of training noise.

3.2. Comparison of infrared-visible image pairs of different quality

The infrared-visible image pairs with high and low informativeness were identified using the proposed CDPC quality assessment method. In this section, the average test accuracies using infrared-visible fusion image pairs of different quality were compared as shown in Figure 7. As described in the experimental setup, the training image pairs are augmented by typical methods, but the fusion image pairs in the test set are fixed. Although image augmentation in conventional computer vision tasks increases the data scale, it inevitably increases information redundancy, wastes training time, and increases power consumption and carbon emissions.

The experimental results have shown clear differences among different selected image pairs in terms of information contributions. Specifically, a higher CDPC score means that the current model has a higher

uncertainty about the image pair, that is, it can bring more meaningful knowledge to the model learning. On the contrary, a low score means that the current model has very high confidence in the image pair and has a good grasp of the pattern and abstract knowledge. Furthermore, random sampling can be considered to be uniform sampling with both high- and low-information-quality. Thus, the average test accuracy performance of high-information-quality image pairs is significantly better than that of random and low-information-quality image pairs. In the case of training with 25% of the whole training set, the test accuracy after training with high-quality samples is 10% higher than that after training with low-quality samples.

3.3. Comparison with other data quality assessment methods

Data quality in this study refers to data characteristics of data such as accuracy, completeness, consistency, timeliness, and reliability. Accuracy represents the consistency of the data with the actual situation, while completeness represents the comprehensiveness of the data. Consistency pertains to whether the data remains consistent across different locations, times, and applications. Timeliness refers to the ability of data to be provided in a timely manner when needed. Reliability relates to the credibility and stability of the data. In this study, data quality is primarily measured by the accuracy of predicted results and the CDPC score obtained using the agreed model.

The proposed CDPC quality assessment method is proved to be able to distinguish image pairs with high- or low-information-quality and realize data-efficient fine-grained photovoltaic hot spot faults recognition. In this section, the comparison with other related works is further carried out to demonstrate the advantage of the proposed CDPC method. The specific experimental settings are consistent and the results are shown in Figure 8.

The above results show that the proposed CDPC method outperforms those in related works in recent years, including coreset (Sener and Savarese, 2017), learning loss (Yoo and Kweon, 2019), feature range (Li and Chao, 2021), and feature mixing (Parvaneh et al., 2022). Better results mean that less training samples are required for the same test accuracy, which means that the proposed CDPC method can select image pairs suitable for efficient learning with richer information diversity.

3.4. Ablation experiment analysis on model structure

After verifying the effectiveness and advancement of the proposed CDPC method, we further carried out ablation experiments to analyze the influence of the model structure. Specifically, the default model structure adopted in this paper was ResNet50, here, the ResNet18 and DenseNet121 were added for comparison. The results are shown in Figure 9.

The performance of the models used in the study exhibits slight variations based on their structures. Deeper models tend to yield better performance, but the consistent differences and trends between high- and low-information-quality image pairs remain evident. It is important to note that, as a data-centric research approach, introducing model differences is not encouraged. Instead, it is recommended to select high-quality data with a fixed model to facilitate efficient learning and obtain reliable results.

3.5. Ablation experiment analysis on feature dimension

In this section, we further conducted the ablation experiments on feature dimension. The dimensionality of the default fusional feature after dimensionality reduction is 256, corresponding to the stage II in Figure 5. Here, we adjusted the threshold setting of PCA dimensionality reduction and set the dimensionality of fusional feature to 128 and 512, respectively. The ablation experimental results are shown in Figure 10.

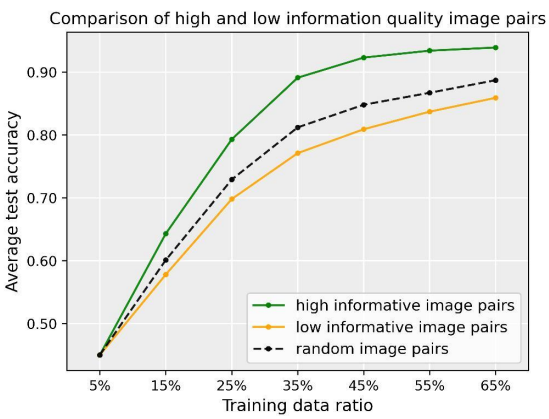

Figure 7. The comparison of infrared-visible image pairs of different quality.

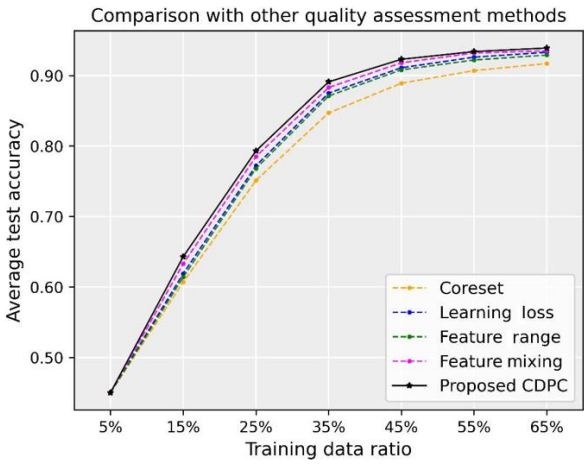

Figure 8. The comparison of infrared-visible image pairs of different quality.

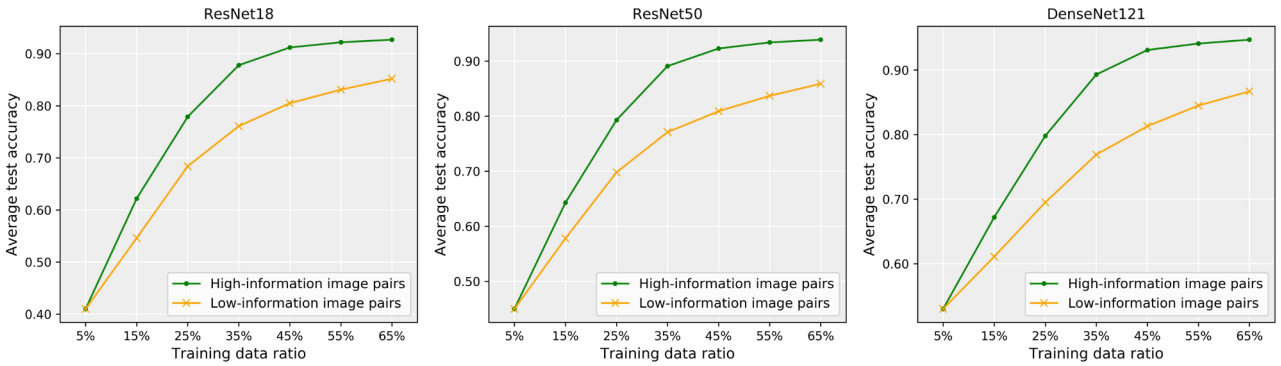

Figure 9. The comparison of infrared-visible image pairs of different quality.

The results show that there should be an information bottleneck in the feature dimension. If the number of feature dimensions is too low, the represented information will be lost. In the case of the same amount of training data, the recognition performance will decline. However, when the number of dimensions increases, the information may be redundant and will not significantly improve the test performance.

4. Discussions

This study explores the research motivation from two perspectives. Firstly, focusing on the agricultural photovoltaic integration development model, we emphasize the investigation of a fine-grained hot spot fault detection method based on infrared-visible image fusion. It is well known that hot spot faults reflect in thermal distribution, exhibiting distinct characteristics in infrared imaging. However, different types of hot spots require specific remedial actions. For instance, dust coverage necessitates cleaning, while component short circuit faults call for replacement. Therefore, fine-grained hot spot identification and analysis are crucial for ensuring the operation of photovoltaic systems and enhancing additional benefits in agricultural photovoltaic integration. Secondly, we specifically study the quality assessment of infrared-visible image pairs. Currently, deep learning-based approaches overlook the influence of data quality, which leads to wastage of training time and data cost while increasing power consumption and carbon emissions.

In this paper, we conducted four main parts of work. Firstly, we collected visible light-infrared image pairs specifically targeting six types of fine-grained hot-spot faults in the agricultural-photovoltaic integration development mode. Additionally, we utilized generative adversarial networks and data augmentation techniques to expand the dataset, resulting in a relatively comprehensive collection of data. Secondly, we developed a fine-grained hot spot fault detection framework based on data quality assessment and information fusion. Within this framework, we proposed a method called combined data

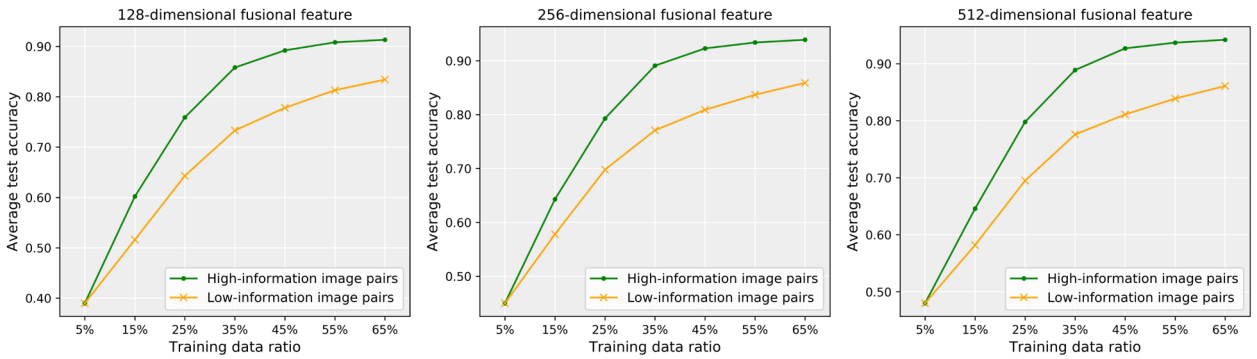

Figure 10. The comparison of infrared-visible image pairs of different quality.

quality and pixel-level consistency (CDPC) for evaluating the information quality of infrared-visible image pairs. Thirdly, we performed extensive experimental analysis to validate the effectiveness and advancement of the proposed methods. Additionally, we conducted ablation experiments to analyze the relevant influencing factors.

The core contributions of this work are the following two points. Firstly, it addresses the lack of research focus on fine-grained hot-spot faults. Most existing studies primarily optimize models using publicly available single infrared photovoltaic (PV) fault datasets. In contrast, we collect and establish an infrared-visible light image pair dataset specifically tailored to the context of agricultural-photovoltaic integration by introducing generative adversarial networks and data augmentation techniques. Building upon this dataset, we propose a hot-spot fault detection framework driven by fine-grained information fusion. Secondly, we propose a novel method to evaluate the information quality of infrared-visible light image pairs, enabling effective differentiation of data quality. These contributions are beneficial for photovoltaic fault type recognition, enhancing detection efficiency and accuracy, and enabling timely maintenance decisions based on fault types.

The current limitations of the work lie in the fact that it adopts a data-centric research approach. Although the use of generative adversarial networks has addressed the issue of insufficient data volume to some extent, it has led to a decrease in the quality of generated data samples. Additionally, the optimization of the model structure has not received sufficient attention. Our future work aims to address these shortcomings by enhancing the quality assessment and selection of the dataset, optimizing the design of lightweight models, and focusing on semantic segmentation tasks.

5. Conclusions

This paper focuses on the fine-grained detection of photovoltaic hot spot faults caused by six different factors in the context of agricultural photovoltaic integration development. The proposed methodology leverages generative adversarial networks and data augmentation techniques to expand the dataset based on a small collected sample. Subsequently, by fusing and reducing the features of infrared and visible light images and evaluating the information quality of the image pairs, an efficient hot-spot fault recognition framework is established. Through extensive experiments, the proposed evaluation method effectively distinguishes the quality of image pairs, reduces data redundancy, and achieves stable hot-spot fault recognition. The results demonstrate that the proposed data evaluation method is not influenced by different network structures, and compressing the fused feature dimensions enables efficient learning. However, excessive compression can lead to the loss of feature information and reduce overall learning effectiveness.

Acknowledgments

This work was supported by the Major Science and Technology Projects of Xinjiang Uygur Autonomous Region (No. 2022A01004-4).

References

Ali MU, Khan HF, Masud M, Kallu KD, Zafar A et al. (2020). A machine learning framework to identify the hotspot in photovoltaic module using infrared thermography. Solar Energy 208: 643-651. https://doi.org/10.1016/j.solener.2020.08.027

Alghazzawi D, Rabie O, Bamasaq O, Albeshri A, Asghar MZ (2022). Sensor-based human activity recognition in smart homes using depthwise separable convolutions. Human-centric Computing and Information Sciences 12: 50. https://doi.org/10.22967/HCIS.2022.12.050

Dhoke A, Sharma R, Saha TK (2020). A technique for fault detection, identification and location in solar photovoltaic systems. Solar Energy, 206: 864-874. https://doi.org/10.1016/j.solener.2020.06.019

Ghosh S, Yadav V K, Mukherjee V (2020). A novel hot spot mitigation circuit for improved reliability of PV module. Institute of Electrical and Electronics Engineers Transactions on Device and Materials Reliability 20 (1): 191-198. https://doi.org/10.1109/TDMR.2020.2970163

Hernández-Callejo L, Gallardo-Saavedra S, Alonso-Gómez V (2019). A review of photovoltaic systems: design, operation and maintenance. Solar Energy 188: 426-440. https://doi.org/10.1016/j.solener.2019.06.017

Khan AA, Laghari AA, Shafiq M, Cheikhrouhou O, Alhakami W et al. (2022). Healthcare ledger management: A blockchain and machine learning-enabled novel and secure architecture for medical industry. Human-centric Computing and Information Sciences 12: 55. https://doi.org/10.22967/HCIS.2022.12.055

Li B, Delpha C, Diallo D, Migan-Dubois A (2021). Application of artificial neural networks to photovoltaic fault detection and diagnosis: a review. Renewable and Sustainable Energy Reviews 138: 110512. https://doi.org/10.1016/j.rser.2020.110512

Li Y, Yang J, Zhang Z, Wen J, Kumar P (2022a). Healthcare data quality assessment for cybersecurity intelligence. Institute of Electrical and Electronics Engineers Transactions on Industrial Informatics 19 (1): 841-848. https://doi.org/10.1109/TII.2022.3190405

Li Y, Nie J, Chao X (2020). Do we really need deep CNN for plant diseases identification? Computers and Electronics in Agriculture 178: 105803. https://doi.org/10.1016/j.compag.2020.105803

Li Y, Chao X (2022). Distance-entropy: an effective indicator for selecting informative data. Frontiers in Plant Science 12: 818895. https://doi.org/10.3389/fpls.2021.818895

Li Y, Chao X, Ercisli S (2022b). Disturbed-entropy: a simple data quality assessment approach. Information and Communication Technology Express 8 (3): 309-312. https://doi.org/10.1016/j.icte.2022.01.006

Li Y, Ercisli S (2023). Explainable human-in-the-loop healthcare image information quality assessment and selection. Chinese Association for Artificial Intelligence Transactions on Intelligence Technology. https://doi.org/10.1049/cit2.12253

Li Y, Chao X (2021). Toward sustainability: trade-off between data quality and quantity in crop pest recognition. Frontiers in Plant Science 12: 811241. https://doi.org/10.3389/fpls.2021.811241

Li J, Hong D, Gao L, Yao J, Zheng K et al. (2022c). Deep learning in multimodal remote sensing data fusion: a comprehensive review. International Journal of Applied Earth Observation and Geoinformation 112: 102926. https://doi.org/10.1016/j.jag.2022.102926

Madhusudana PC, Birkbeck N, Wang Y, Adsumilli B, Bovik A C (2022). Image quality assessment using contrastive learning. Institute of Electrical and Electronics Engineers Transactions on Image Processing 31: 4149-4161. https://doi.org/10.1109/TIP.2022.3181496

Malik A, Haque A, Kurukuru VB, Khan MA, Blaabjerg F. (2022). Overview of fault detection approaches for grid connected photovoltaic inverters. e-Prime-Advances in Electrical Engineering, Electronics and Energy 2: 100035. https://doi.org/10.1016/j.prime.2022.100035

Nie J, Wang Y, Li Y, Chao, X (2022a). Artificial intelligence and digital twins in sustainable agriculture and forestry: a survey. Turkish Journal of Agriculture and Forestry, 46 (5): 642-661. https://doi.org/10.55730/1300-011X.3033

Nie J, Wang Y, Li Y, Chao X (2022b). Sustainable computing in smart agriculture: survey and challenges. Turkish Journal of Agriculture and Forestry 46 (4): 550-566. https://doi.org/10.55730/1300-011X.3025

Patil RR, Kumar S (2022). Rice-fusion: a multimodality data fusion framework for rice disease diagnosis. Institute of Electrical and Electronics Engineers Access 10: 5207-5222. https://doi.org/10.1109/ACCESS.2022.3140815

Parvaneh A, Abbasnejad E, Teney D, Haffari GR, Van Den Hengel A et al. (2022). Active learning by feature mixing. Proceedings of the International Conference on Computer Vision Conference on Computer Vision and Pattern Recognition 12227-12236. https://doi.org/10.1109/CVPR52688.2022.01192

Su B, Chen H, Liu K, Liu W (2021). RCAG-Net: Residual channelwise attention gate network for hot spot defect detection of photovoltaic farms. Institute of Electrical and Electronics Engineers Transactions on Instrumentation and Measurement 70: 1-14. https://doi.org/10.1109/TIM.2021.3054415

Schlett T, Rathgeb C, Henniger O, Galbally J, Fierrez J et al. (2022). Face image quality assessment: A literature survey. Association for Computing Machinery Computing Surveys 54 (10s): 1-49. https://doi.org/10.1145/3507901

Sener O, Savarese S (2017). Active learning for convolutional neural networks: A core-set approach. arXiv preprint arXiv 1708.00489. https://doi.org/10.48550/arXiv.1708.00489

Sovacool BK, Griffiths S (2020). The cultural barriers to a low-carbon future: a review of six mobility and energy transitions across 28 countries. Renewable and Sustainable Energy Reviews 119: 109569. https://doi.org/10.1016/j.rser.2019.109569

Tang L, Yuan J, Ma J (2022). Image fusion in the loop of high-level vision tasks: a semantic-aware real-time infrared and visible image fusion network. Information Fusion 82: 28-42. https://doi.org/10.1016/j.inffus.2021.12.004

Wang A, Xuan Y (2021). Close examination of localized hot spots within photovoltaic modules. Energy Conversion and Management 234: 113959. https://doi.org/10.1016/j.enconman.2021.113959

Xie Y, Yu B, Lv S, Zhang C, Wang G et al. (2021). A survey on heterogeneous network representation learning. Pattern Recognition 116: 107936. https://doi.org/10.1016/j.patcog.2021.107936

Yang J, Lan G, Li Y, Gong Y, Zhang Z et al. (2022a). Data quality assessment and analysis for pest identification in smart agriculture. Computers and Electrical Engineering 103: 108322. https://doi.org/10.1016/j.compeleceng.2022.108322

Yang J, Zhang Z, Xiao S, Ma S, Li Y et al. (2023a). Efficient data-driven behavior identification based on vision transformers for human activity understanding. Neurocomputing 530: 104-115. https://doi.org/10.1016/j.neucom.2023.01.067

Yang J, Yang Y, Li Y, Zhang Z, Wen J (2023b). Image quality assessment via inter-class and intra-class differences for efficient classification. Neural Processing Letters 55 (9):12169-81. https://doi.org/10.1007/s11063-023-11414-x

Yang Y, Li Y, Yang J, Wen J (2022b). Dissimilarity-based active learning for embedded weed identification. Turkish Journal of Agriculture and Forestry 46 (3): 390-401. https://doi.org/10.55730/1300-011X.3011

You X, Yang L, Zhou X, Zhang Y (2022). Sustainability and carbon neutrality trends for microalgae-based wastewater treatment: a review. Environmental Research 209: 112860. https://doi.org/10.1016/j.envres.2022.112860

Yoo D, Kweon IS (2019). Learning loss for active learning. Proceedings of the International Conference on Computer Vision Conference on Computer Vision and Pattern Recognition 93-102. https://doi.org/10.1109/CVPR.2019.00018

Zhang H, Xu H, Tian X, Jiang J, Ma J (2021). Image fusion meets deep learning: a survey and perspective. Information Fusion 76: 323-336. https://doi.org/10.1016/j.inffus.2021.06.008